Chemistry–A European Journal
Research Article
doi.org/10.1002/chem.202300174
Chemistry Europe
European Chemical Societies Publishing
www.chemeurj.org

Comprehensive Investigation of Anion Species in Crystalline Li^+ ion Conductor $Li_{27-x}[P_4O_{7+x}N_{9-x}]O_3$ ($x \approx 1.9(3)$)

Stefanie Schneider,[a] Eva-Maria Wendinger,[a] Volodymyr Baran,[b] Anna-Katharina Hatz,[a, c] Bettina V. Lotsch,[a, c] Markus Nentwig,[d] Oliver Oeckler,[d] Thomas Bräuniger,[a] and Wolfgang Schnick*[a]

Abstract: The Li^+ ion conductor $Li_{27-x}[P_4O_{7+x}N_{9-x}]O_3$ ($x \approx 1.9$) has been synthesized from P_3N_5, Li_3N and Li_2O in a Ta ampoule at 800 °C under Ar atmosphere. The cubic compound crystallizes in space group $I\bar{4}3d$ with $a = 12.0106(14)$ Å and $Z = 4$. It contains both non-condensed $[PO_2N_2]^{5-}$ and $[PO_3N]^{4-}$ tetrahedra as well as O^{2-} ions, surrounded by Li^+ ions. Charge neutrality is achieved by partial occupancy of Li positions, which was refined with neutron powder diffraction data. Measurements of the partial ionic and electronic conductivity show a total ionic conductivity of 6.6×10^{-8} S cm^{-1} with an activation energy of 0.46 ± 0.02 eV and a bulk ionic conductivity of 4×10^{-6} S cm^{-1} at 25 °C, which is close to the ionic conductivity of amorphous lithium nitridophosphate. This makes $Li_{27-x}[P_4O_{7+x}N_{9-x}]O_3$ an interesting candidate for investigation of structural factors affecting ionic conductivity in lithium oxonitridophosphates.

Introduction

Introduction of nitrogen into oxide glasses was found to affect materials properties significantly.[1] Therefore, oxonitrides became the subject of thorough investigations.[2–6] Especially oxonitridophosphates showed promising alterations of their properties compared to oxosilicate and oxophosphate glasses.[4,6,7] The initial focus on materials properties such as chemical durability, softening temperature, refractive index, or thermal expansion[4,8] has more recently been shifted toward electronic properties such as ionic or electronic conductivity.[9–11] Amorphous lithium phosphorus oxonitride (LiPON) materials with a composition of $Li_xPO_yN_z$ have become a hot topic due to their relatively high Li^+ ion conductivity, paired with high electrochemical inertness.[12] Although these materials have been thoroughly investigated focusing on application as solid electrolytes, the underlying conduction mechanism is largely unknown. Structural investigation on glasses, such as amorphous LiPON, is difficult with standard techniques such as X-ray diffraction (XRD). However, applying analytical tools for local order such as solid-state NMR (ssNMR) allows the assessment of structural features such as the N content and N positions as well as the degree of condensation of $P(O,N)_4$ tetrahedra that have a significant influence on the conductivity and other materials properties.[8,13–18] ssNMR enables characterization of both amorphous and crystalline materials and ^{31}P ssNMR proved to be a suitable tool to detect the composition of PO_yN_{4-y} tetrahedra, since the chemical shift is highly dependent on the O/N ratio.[14–17,19]

In addition, modelling of ionic diffusion pathways is also challenging and requires complex structural models based on crystalline frameworks.[20] These crystalline model structures help to understand the influence of certain structural features on Li^+ conductivity, as they provide an ordered environment in which various influences can be observed.

To date, only few crystalline lithium oxonitridophosphates are known and thus the number of model structures is limited. They show a high anionic structural diversity including non-condensed PO_yN_{4-y} with $1 \leq y \leq 4$ tetrahedra and one-dimensionally connected chains of tetrahedra. Recently, $Li_{5+x}P_2O_{6-x}N_{1+x}$ with pairs of corner-sharing tetrahedra $[P_2O_6N]^{5-}$ with a bridging N atom has been reported.[21] Crystalline lithium

[a] S. Schneider, Dr. E.-M. Wendinger, Dr. A.-K. Hatz, Prof. Dr. B. V. Lotsch, Dr. T. Bräuniger, Prof. Dr. W. Schnick
Department of Chemistry
University of Munich (LMU)
Butenandtstr. 5–13 (D), 81377 Munich (Germany)
E-mail: wolfgang.schnick@uni-muenchen.de
[b] Dr. V. Baran
Heinz Maier-Leibnitz Zentrum
Technical University of Munich, FRM II
Lichtenbergstr. 1 (D), 85748 Garching (Germany)
and
Deutsches Elektronen-Synchrotron DESY
Notkestr. 85, 22607 Hamburg (Germany)
[c] Dr. A.-K. Hatz, Prof. Dr. B. V. Lotsch
Max Planck Institute for Solid State Research
Heisenbergstr. 1 (D), 70569 Stuttgart (Germany)
[d] Dr. M. Nentwig, Prof. Dr. O. Oeckler
Fakultät für Chemie und Mineralogie
Institut für Mineralogie, Kristallographie und Materialwissenschaft
Scharnhorststr. 20 (D), 04275 Leipzig (Germany)

Supporting information for this article is available on the WWW under https://doi.org/10.1002/chem.202300174

oxonitridophosphates are lithium ion conductors and their conductivities range from 1×10^{-13} to 6.0×10^{-8} S cm^{-1} (Table 3).[22–26]

In this work, we report on synthesis, structural characteristics and Li^+ ion conductivity of $Li_{27-x}[P_4O_{7+x}N_{9-x}]O_3$. Similar to $Li_{14}(PON_3)_2$, $Li_{27-x}[P_4O_{7+x}N_{9-x}]O_3$ is composed of non-condensed $P(O,N)_4$ tetrahedra and O^{2-} ions.[24] The range of anionic species in this compound make it a valuable model system for the investigation of the impact of structural features on Li^+ ion conductivity in LiPON compounds.

Results and Discussion

Synthesis

The title compound was initially observed in a heterogeneous sample of partially hydrolyzed $Li_{10}P_4N_{10}$. Targeted synthesis was subsequently accomplished from Li_3N, P_3N_5, and Li_2O. Stoichiometric mixtures of starting materials as shown in the idealized reaction Equation (1) did not yield $Li_{27-x}[P_4O_{7+x}N_{9-x}]O_3$, but $Li_{5+x}P_2O_{6-x}N_{1+x}$.[21] Instead, Li_3N had to be used in excess to form a Li_3N flux, a method previously reported for synthesis of lithium nitridophosphates.[27–31] The reaction mixture was heated to 800 °C for 90 h under Ar atmosphere in an open Ta crucible placed in a fused silica ampoule.

$$(7-3x)\ Li_3N + 4\ P_3N_5 + (30+3x)\ Li_2O \rightarrow 3\ Li_{27-x}[P_4O_{7+x}N_{9-x}]O_3 \quad (1)$$

Despite comprehensive variation of the stoichiometry of starting materials and reaction conditions, a phase-pure product could not be achieved so far. Similar to the synthesis of lithium nitridophosphates, Li_3P is formed as a side product.[31] Other identified side phases include $Li_{10}P_4N_{10}$, $Li_5P_2O_6N$, and Li_2O.[21,30] Whereas the quantity of these side phases could be lowered by prolonged reaction times, a small amount of Li_2O remained in all samples. In contrast, the Li_3P content increased upon prolonged reaction times and higher temperatures, but this byproduct was removed with dry EtOH. Longer treatment of the sample with EtOH also decreases the amount of Li_2O. A moisture- and air-sensitive, colorless, microcrystalline powder was obtained. Subsequently, analytical data were collected on a sample with 11 wt-% Li_2O as side phase, as determined by Rietveld refinement (measurements were taken with Cu $K_{\alpha1}$ radiation, Figure 1).

By ampoule synthesis, only relatively small amounts of the product could be synthesized (batches up to 200 mg). Experiments in a hot isostatic press (HIP) could enable larger batch sizes, however, no phase pure synthesis could be achieved with this method, either.

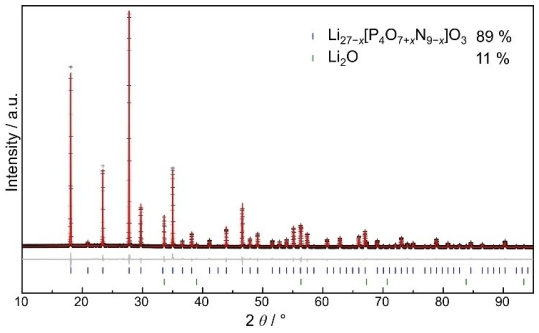

Figure 1. Observed (black crosses, Cu $K_{\alpha1}$ radiation) and calculated (red line) powder diffraction pattern of $Li_{27-x}[P_4O_{7+x}N_{9-x}]O_3$. Calculated Bragg reflections for $Li_{27-x}[P_4O_{7+x}N_{9-x}]O_3$ and Li_2O are shown with blue and green markers, respectively.

Crystal structure determination

X-ray diffraction

The structure model of $Li_{27-x}[P_4O_{7+x}N_{9-x}]O_3$ was determined by single-crystal X-ray diffraction, applying direct methods. Due to small crystallite sizes of less than 10 μm, diffraction data were collected at the ESRF beamline ID11 in Grenoble. The title compound crystallizes in cubic space group $I\bar{4}3d$ with $a=12.0106(14)$ Å and $Z=4$. The analysis showed that the structure consists of anionic $P(O,N)_4$ tetrahedra with only one crystallographically independent P site. Additional O^{2-} and Li^+ make this compound a lithium oxonitridophosphate oxide (Figure 3).

Assuming all Li and oxide positions being fully occupied and a mixed occupancy of O and N positions in $P(O,N)_4$ tetrahedra leads to the charge-neutral sum formula of $Li_{27}[P_4O_7N_9]O_3$. Written in brackets is the composition of tetrahedra, O from oxide positions is given outside of the brackets. As deduced from ssNMR data, there are both $[PO_3N]^{4-}$ and $[PO_2N_2]^{5-}$ tetrahedra present in the structure. Due to the similar electron counts, O and N lack X-ray scattering contrast so that ordering of O and N atoms cannot be assessed. The charge neutral sum formula mentioned above seems not fully consistent with these types of tetrahedra. With the mixed occupancy observed in neutron diffraction, charge neutrality can only be reached with Li vacancies, resulting in the sum formula $Li_{27-x}[P_4O_{7+x}N_{9-x}]O_3$ (see below).

Solid-state magic angle spinning NMR spectroscopy

In principle, five different $[PO_yN_{4-y}]^{(7-y)-}$ ($y=0-4$) tetrahedra are possible. To find out which particular tetrahedral anions are present, ^{31}P solid-state magic angle spinning (MAS) NMR was performed.

Although there is only one crystallographic P site in the average structure, ^{31}P MAS NMR (Figure 2) shows two signals with a ratio of 72 to 28% at chemical shifts of 33.0 and 19.6 ppm, respectively, suggesting two different atomic environments for P. At 44 ppm, the intensity is raised slightly above

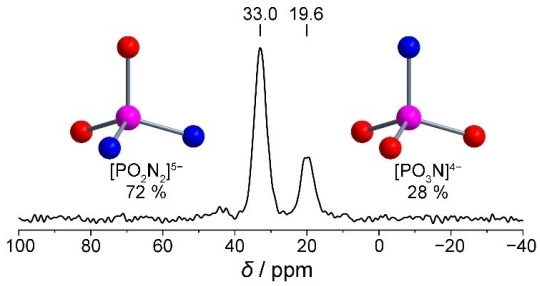

Figure 2. ^{31}P NMR spectrum of $Li_{27-x}[P_4O_{7+x}N_{9-x}]O_3$ at a MAS rate of 25 kHz. Two signals are visible at 33.0 and 19.6 ppm, which belong to the P1 atomic position in the $[PO_2N_2]^{5-}$ and the $[PO_3N]^{4-}$ environment, respectively (P: pink, O: red, N: blue).

the background, which might indicate presence of a small amount of another different chemical environment around P. However, the intensity of the signal was too small for integration, so no ratio could be obtained. A ^{31}P–^{31}P 2D double-quantum single-quantum correlation MAS NMR spectrum confirms that both signals are from the same phase (Figure S7 in Supporting Information).

Previous NMR studies on LiPON materials have shown a shift in the positions of ^{31}P MAS NMR signals of approximately +10 ppm for each O atom that is replaced by N within non-condensed $P(O,N)_4$ tetrahedra.[16] Table 1 shows ^{31}P MAS NMR shifts for lithium oxonitridophosphates with discrete $P(O,N)_4$ tetrahedra. The two signals of the title compound are in good agreement with literature data of $[PO_2N_2]^{5-}$ (31.3 ppm)[25] and $[PO_3N]^{4-}$ tetrahedra (19.8 and 19.4 ppm)[16,25] (Figure 2). However, the presence of $[PO_2N_2]^{5-}$ and $[PO_3N]^{4-}$ in a 72:28 ratio would not meet the number of negative charges required for a charge-neutral sum formula with the Li positions found with X-ray diffraction fully occupied (−5.25 per P atom, balancing 27 positive charges from Li^+ and six negative charges from O^{2-}). Charge neutrality with a partial sum formula of $4\times[(PO_2N_2)_{0.72}(PO_3N)_{0.28}]^{4.72-}$, as derived from NMR would result in too few negative charges to balance the charges from fully occupied Li positions. To achieve charge neutrality, there are two options. One possibility is a mixed occupancy of the oxide position with N, so a higher negative charge would result. The second possibility are Li vacancies, which would lower the amount of positive charges and then result in $x=2.12$. Furthermore, the weak resonance at 44 ppm might indicate the presence of $[PON_3]^{6-}$ (Figures S3 and S4). This would further reduce the value of x. The $[PO_2N_2]^{5-}$ and $[PO_3N]^{4-}$ tetrahedra may be distributed randomly. Alternatively, some form of ordering might decrease the symmetry to the space groups $R3c$ or $I\bar{4}2d$. No splitting of reflections is observed in either X-ray or neutron powder diffraction. Refinement was attempted in other space groups, but did not yield indication towards lowering of symmetry.

Table 1. Overview of ^{31}P MAS NMR shifts for non-condensed lithium phosphates.

$[PO_yN_{4-y}]^{(7-y)-}$	Compound	δ / ppm
$[PN_4]^{7-}$	Li_7PN_4	49.2, 54.6[28]
$[PON_3]^{6-}$	$Li_{14}(PON_3)_2O$	44.3[24]
$[PO_2N_2]^{5-}$	$Li_{3.6}PO_{3.4}N_{0.6}$	31.3[25]
$[PO_3N]^{4-}$	$Li_{3.6}PO_{3.4}N_{0.6}$, a-LiPON[a]	19.8[25], 19.4[16]
$[PO_4]^{3-}$	$Li_{3.6}PO_{3.4}N_{0.6}$, a-LiPON[a], Li_3PO_4	10.3[25], 9.3[16], 8.9[32]

[a] amorphous LiPON with 2.5 at-% N.

^{6}Li ($\delta=1.9$ ppm) and ^{7}Li ($\delta=2.8$ ppm) MAS NMR both show only one signal, which is probably due to significant Li^+ ion mobility (Figures S5 and S6) and the three crystallographically independent sites cannot be distinguished. However, the signals exhibit shoulders due to slightly different local environments. The chemical shift is in good agreement with known shifts of lithium, which range from 4.9 to 1.6 ppm in lithium (oxo)nitridophosphates.[24,27,28,30,31]

Neutron powder diffraction

Ordering of O and N atoms and thus $[PO_2N_2]^{5-}$ and $[PO_3N]^{4-}$ might result in reduced space group symmetry. Charge neutrality could be achieved by Li vacancies or mixed occupancy of the O3 position with N. To address these questions, neutron diffraction data were obtained (Figure S2). Since only small amounts of the product could be obtained in one batch and with respect to the large amount of sample needed for neutron diffraction, a combined sample with Li_2O (16%) and $Li_{5+x}P_2O_{6-x}N_{1+x}$ (9%) as side phases was used. The data in Figure S2 show no split reflections and thus no indication of a decrease in symmetry towards subgroups of $I\bar{4}3d$ by ordering of the O/N positions. Neutron data suggest statistically occupied O/N positions in tetrahedra. The O1/N1 position is predominantly occupied by oxygen (81(3) %), whereas the O2/N2 position shows no preferred occupancy (53(3) % N). The O3 position is fully occupied with O as expected for a position that is not part of a phosphate ion (Figure 3). The resulting Li site occupancy of 92.9(12) % leads to the sum formula $Li_{27-x}[P_4O_{7+x}N_{9-x}]O_3$ with $x\approx1.9(3)$, which is close to the value derived from NMR ($x=2.12$), if only $[PO_3N]^{4-}$ and $[PO_2N_2]^{5-}$ are assumed. As mentioned before, the value obtained from NMR might be lower, if $[PON_3]^{6-}$ is indeed present. Within the margin of error, the values are congruent. Thus, $x\approx1.9(3)$, as obtained from neutron diffraction, will be used for further considerations.

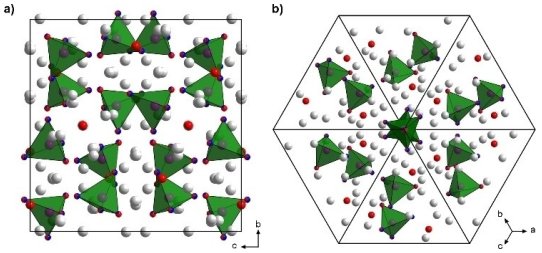

Figure 3. Unit cell of $Li_{27-x}[P_4O_{7+x}N_{9-x}]O_3$ along [1 0 0] (a) and [1 1 1] (b) (P: pink, O: red, N: blue, Li: light gray.

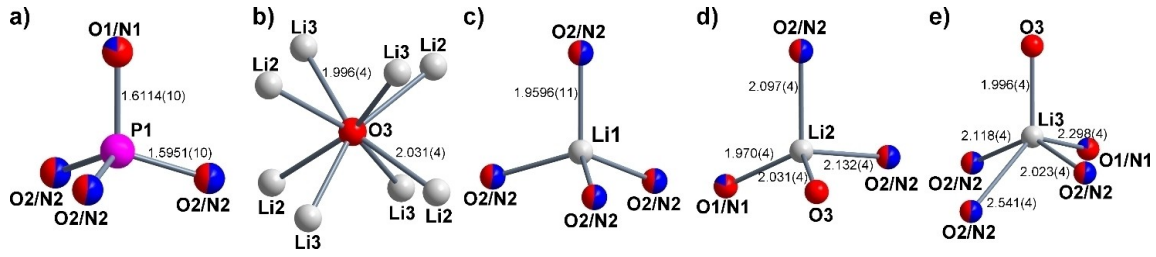

Figure 4. Coordination of different atomic positions with bond lengths in Å (P: pink, O: red, N: blue, Li: light gray).

Combined structure model

Analytical data are consistent with the space group $I\bar{4}3d$ for $Li_{27-x}[P_4O_{7+x}N_{9-x}]O_3$ ($x \approx 1.9(3)$); crystallographic data are summarized in Table 2. Atomic coordinates and anisotropic displacement parameters as well as selected interatomic distances and angles are listed in Tables S1 to S4. The unit cell is shown in Figure 3.

There is one crystallographic P position which is tetrahedrally coordinated by one O1/N1 position and three symmetry equivalent O2/N2 positions with O/N disorder on both positions according to neutron diffraction. Thus, $[PO_2N_2]^{5-}$ and $[PO_3N]^{4-}$, as confirmed by NMR are statistically distributed. The final structure model is based on SCXRD but uses site occupancies from neutron powder diffraction without further refinement. P–O/N bond lengths in lithium oxonitridophosphates are assumed to be longer than pure P–O bonds and shorter than pure P–N bonds, due to the larger ionic radius of N^{3-} in contrast to O^{2-} and stronger covalency of the P–N bond.[22,33,34] Despite the mixed occupancy bond lengths in $Li_{27-x}[P_4O_{7+x}N_{9-x}]O_3$ can be best compared to lithium ortho-oxonitridophosphates, Li_7PN_4, or Li_3PO_4. Comparison to $Li_{14}(PON_3)_2O$ proves useful, since it also contains oxide ions.[22,24,25,35,36] P–O bond lengths in Li_3PO_4 range from 1.53 to 1.58 Å,[36] whereas P–N bond lengths in Li_7PN_4 are within a range of 1.69 to 1.73 Å.[35] Thus, P–O/N bond lengths in $Li_{27-x}[P_4O_{7+x}N_{9-x}]O_3$ with 1.6114(10) Å (P1–O1/N1) and 1.5951(10) Å (P1–O2/N2) are in good agreement with other lithium (nitrido-)phosphates.[22–25,27,28,30,31,35,36]

The oxide ion O^{2-} (O3 position) shows a distorted cubic coordination by eight Li^+ positions (Li2 and Li3). Two of the three Li positions are tetrahedrally coordinated by O/N atoms. Li3 is located in a distorted tetragonal pyramid (Figure 4). Neutron data shows Li vacancies (92% occupancy) Pure Li–O distances are in the range of 1.996(4) Å to 2.029(3) Å, whereas Li–O/N distances range from 1.9595(12) Å to 2.299(6) Å, which is in good agreement with known Li–O and Li–N distances.[27–31,36–39] All Li-centered polyhedra share edges with other Li-centered polyhedra, which decreases the Li–Li distances, enabling potentially higher conductivity as discussed below.

Table 2. Crystallographic data of $Li_{27-x}[P_4O_{7+x}N_{9-x}]O_3$ ($x \approx 1.9$) from single-crystal X-ray diffraction data.

Crystal size [mm]	$0.01 \times 0.01 \times 0.03$
Formula	$Li_{27-x}[P_4O_{7+x}N_{9-x}]O_3$
Formula weight [g mol^{-1}]	587.78
Crystal system	cubic
Space group	$I\bar{4}3d$ (no. 220)
Lattice parameter a [Å]	12.0106(14)
Cell volume [Å^3]	1732.6(6)
Formula units per unit cell	4
Density [g·cm^{-3}]	2.253
μ [mm^{-1}]	0.071
Radiation [λ/Å]	Synchrotron, $\lambda = 0.29470$ Å
θ-range [°]	$1.7 \leq \theta \leq 13.7$
Total no. of reflections	17851
Independent reflections	691, thereof 687 with $F^2 > 2\sigma(F^2)$
Refined parameters	38
R_{int}; R_σ	0.0607; 0.0182
$R1$ (all data); $R1$ ($F^2 > 2\sigma(F^2)$)	0.0197; 0.0194
$wR2$ (all data); $wR2$ ($F^2 > 2\sigma(F^2)$)	0.0512; 0.0511
Goodness of fit (χ^2)	1.177
$\Delta\rho_{max}$; $\Delta\rho_{min}$/e·Å^{-3}	0.212; −0.151

FTIR and chemical analysis

The infrared spectrum shows no vibrational modes of O–H and N–H bonds in the range of 2800–3200 and 3000–3500 cm^{-1}, respectively (Figure 5). Thus, no N–H or O–H bonds are present in the structure. The five distinct signals at 1050, 1000, 940, 835, and 785 cm^{-1} may be attributed to P–O stretching modes that are typically found between 900 and 1200 cm^{-1}, whereas O–P–O bending modes occur around 650–300 cm^{-1}.[40] The broad signal around 400 cm^{-1} might be caused by Li cation vibrations.[41]

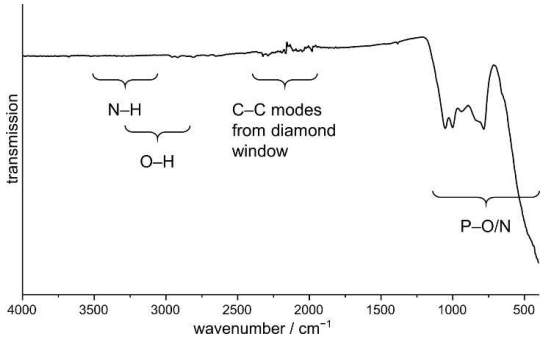

Figure 5. IR spectrum of $Li_{27-x}[P_4O_{7+x}N_{9-x}]O_3$. No signals are visible in the area of 3000–3500 cm^{-1}. Thus, no N–H or O–H bonds are present in the structure. Increased background in the area 2300–2000 cm^{-1} is due to C–C bonds in the diamond window of the ATR unit.

Elemental analysis is complicated by the fact that the samples are prone to hydrolysis and the presence of side phases. Energy-dispersive X-ray (EDX) spectroscopy cannot precisely quantify light elements, especially Li. Thus, elemental analyses only indicated that no other elements are present (Tables S8 and S9).

Thermal stability

The thermal stability of $Li_{27-x}[P_4O_{7+x}N_{9-x}]O_3$ was investigated using a sample with 11 % Li_2O for temperature-dependent X-ray powder diffraction. Up to 620 °C, the reflections of $Li_{27-x}[P_4O_{7+x}N_{9-x}]O_3$ only show the expected thermal shift. At 640 °C, possibly as a result of a reaction between $Li_{27-x}[P_4O_{7+x}N_{9-x}]O_3$ and the present impurity Li_2O, $Li_{5+x}P_2O_{6-x}N_{1+x}$ is formed. At 860 °C, reflections of Li_3PO_4 indicate decomposition. Above 880 °C, full decomposition has taken place and reflections of neither $Li_{5+x}P_2O_{6-x}N_{1+x}$ nor $Li_{27-x}[P_4O_{7+x}N_{9-x}]O_3$ are detectable (Figure S8).

Ionic and electronic partial conductivities

For a cold pressed pellet of $Li_{27-x}[P_4O_{7+x}N_{9-x}]O_3$ with 11 % of Li_2O as side phase, a total ionic conductivity of 6.6×10^{-8} S cm^{-1} at 25 °C with an activation energy of 0.46 ± 0.02 eV (extrapolated to 3.8×10^{-6} S cm^{-1} at 127 °C) and a bulk ionic conductivity of 4×10^{-6} S cm^{-1} were measured by electrochemical impedance spectroscopy. The impedance spectrum in Figure 6 consists of three contributions: one high frequency and one low frequency semicircle and a spike at low frequencies. The semicircles are modelled by a resistor R and a constant phase element (CPE) in parallel denoted as R1-CPE1 and R2-CPE2, respectively.

The low frequency spike stems from the polarization of Li^+ ions at the blocking electrode and is modelled by a CPE (CPE3) in series. The total ionic conductivity is calculated by $\sigma = d/AR_{tot}$ with d being the thickness of the pellet, A the surface area and R_{tot} the sum of R1 and R2 that were obtained from the fit of the spectrum. Considering the effective capacitances (C_{eff}) of the two processes of 24 pF for the high frequency semicircle and 0.1 nF for the low frequency semicircle, they are assigned to bulk and grain boundary contributions, respectively.[42] The C_{eff} is calculated by $C_{eff} = (Q/(R^{\alpha-1}))^{1/\alpha}$ with Q being CPE's admittance value, R the respective resistance in parallel to the CPE and α a fitting parameter with a value between 0.5 and 1, modelling the deviation from an ideal capacitor. An activation energy E_a of 0.46 ± 0.02 eV is derived from the total conductivity by $\sigma = (\sigma_0/T)\cdot e^{-E_A/RT}$ from heating and cooling the sample as plotted in Figure 6b. This activation energy represents an overlapped value of the two processes, which is dominated by the more resistive grain boundary process. The issue of reproducibility is discussed in the Supporting Information (Figure S9, Table S10).

The average activation energy is lower with 0.39 ± 0.03 eV being consistent with the less pronounced influence of the resistive grain boundaries in this sample (Table S10). An electronic conductivity of 9×10^{-10} S cm^{-1} of $Li_{27-x}[P_4O_{7+x}N_{9-x}]O_3$ was obtained by potentiostatic polarization measurements as depicted in Figure S9, leading to a transference number $\tau_i = \sigma_{ion}/(\sigma_{ion} + \sigma_{eon})$ of 0.991, rendering $Li_{27-x}[P_4O_{7+x}N_{9-x}]O_3$ a predominantly ionic conductor.

The total ionic conductivity of $Li_{27-x}[P_4O_{7+x}N_{9-x}]O_3$ at 80 °C (Table 3) is comparable to Li_2PO_2N, but is lower than that of amorphous a-LiPON with 2.5 at-% of N at room temperature. Li_2O is contained in the sample as side phase (11 %) and is considered to exist side by side to the title phase. As Li_2O exhibits a Li^+ ion conductivity well below that of $Li_{27-x}[P_4O_{7+x}N_{9-x}]O_3$ (10^{-12} S cm^{-1}),[44] its effect on the total conductivity should only be negative. The effect should be comparable to that of a lower relative density of the pellet, resulting in a larger total resistance. Nevertheless, the bulk ionic conductivity of 4×10^{-6} S cm^{-1} is very similar to amorphous a-LiPON.

Lacivita et al. have performed diffusivity simulations on amorphous model systems to investigate structural features that are beneficial or detrimental for ionic conductivity.[18] At

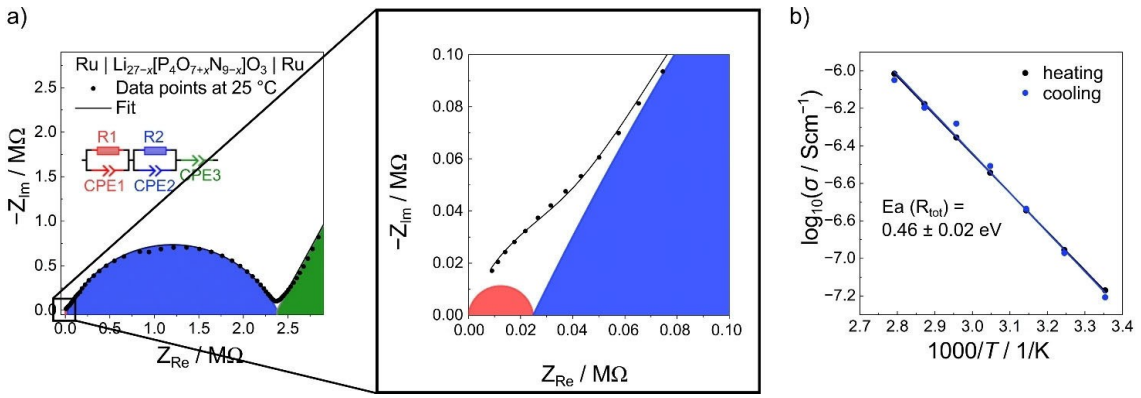

Figure 6. a) Impedance spectrum of $Li_{27-x}[P_4O_{7+x}N_{9-x}]O_3$ with 11 % Li_2O as side phase, showing two semicircles of the bulk (R1-CPE1) and grain boundary process (R2-CPE2), respectively. The activation energy of the total ionic conductivity from heating and cooling the sample determined in b) is 0.46 ± 0.02 eV and is dominated by the grain boundary process.

Table 3. Ionic conductivity and activation energy of lithium oxonitridophosphates.

Compound	σ at 25 °C [S cm^{-1}]	σ at 80 °C [S cm^{-1}]	σ at 127 °C [S cm^{-1}]	E_a [eV]	Ref.
$Li_{27-x}[P_4O_{7+x}N_{9-x}]O_3$ (best sample)	$\sigma_{tot} = 6.6\times10^{-8}$	7.9×10^{-7}	3.8×10^{-6}[a]	0.46	This work
$Li_{27-x}[P_4O_{7+x}N_{9-x}]O_3$	$\sigma_{tot} = 1.4\times10^{-7}$	1.3×10^{-6}	5.6×10^{-6}[a]	0.39	This work
a-LiPON	1.6×10^{-6}			0.58	[43]
$Li_{2.88}PO_{3.73}N_{0.14}$	1×10^{-13}			0.97	[22]
Li_2PO_2N		8.8×10^{-7}		0.57	[23]
$Li_{14}(PON_3)_2O$					[24]
$Li_{3.6}PO_{3.4}N_{0.6}$	5.6×10^{-8}			0.55	[25]
$Li_{5+x}P_2O_{6-x}N_{1+x}$	$\sigma_{tot} = 4.6\times10^{-8}$			0.52	[21]

[a] Extrapolated values.

first glance, the conductivity of $Li_{27-x}[P_4O_{7+x}N_{9-x}]O_3$ might seem high, considering that there are several features present in the structure that have been associated with reduced ionic conductivity.

For example, the presence of connected $P(O,N)_4$ tetrahedra that share a bridging N (N_d) would be advantageous in comparison to the non-connected $P(O,N)_4$ tetrahedra found in the structure. This is due to the overall reduced anion charge of $[P_2O_6N]^{5-}$ in comparison to two $[PO_4]^{3-}$ that exerts smaller coulombic attraction on Li^+ and thereby enables higher Li^+ mobility. Instead of these beneficial double tetrahedra, the structure contains even more highly charged $[PO_3N]^{4-}$ and $[PO_2N_2]^{5-}$, as well as isolated O^{2-} that was also shown to decrease Li^+ ion mobility due to larger electrostatic interaction.[18,45]

Additionally, edge-sharing between $Li(O,N)_4$ and $P(O,N)_4$ improves conductivity, as the close proximity between Li and P destabilizes Li sites. In $Li_{27-x}[P_4O_{7+x}N_{9-x}]O_3$ however, $Li(O,N)_4$ and $P(O,N)_4$ tetrahedra only share corners. Only the polyhedron around Li3 shares edges with two $P(O,N)_4$ tetrahedra. As no other coordination geometry than tetrahedra are discussed for this substance class in literature, the influence of other polyhedra is not known. However, as the effect is based on coulombic repulsion between P and Li, and larger polyhedra cause larger distances between the two atoms, no or only slight destabilization of Li sites by the proximity to P might be present.

Finally, amorphization of structures is known to increase Li^+ mobility significantly. As the presence of defects flatten the energy landscape around Li, amorphous compounds often have higher conductivities than crystalline materials.[18,45–47] Thus, a lower conductivity of crystalline LiPON in comparison to amorphous a-LiPON is expected.

Summarizing, several structural features seem to be detrimental for the Li^+ ion conductivity in $Li_{27-x}[P_4O_{7+x}N_{9-x}]O_3$ at first glance. However, on a second look, there are several structural features that could be beneficial for the Li^+ ion conductivity.

Firstly, partial occupancy of Li sites opens migration pathways. In a fully occupied crystal with no defects, no mobility is possible. Holzwarth et al. have calculated for Li_3PO_4 that the activation energy consists to a large part of the formation of interstitial and site defects, whereas migration barriers play only a minor role. Thus, the observed vacancies might be essential for Li^+ mobility.[46]

Additionally, the density of Li^+ in the structure is very high, which might result in coulombic repulsion and thus destabilization of Li positions by neighboring Li. Whereas no edge-sharing is observed with $P(O,N)_4$ tetrahedra, which would destabilize Li positions, there are many $Li(O,N)_4$ sharing edges with other $Li(O,N)_4$ polyhedra. Lacivita et al. stated that a high number of short-range Li–Li interactions might lead to higher conductivity due to raised Li site energies. Around each Li position are a minimum of six edge-sharing $Li(O,N)_4$ polyhedra. This is also represented in the number of next Li neighbors with a distance of 3 Å around each Li site, which is 8 (Li1), 8 (Li2), and 6 (Li3). This is a very large number of direct Li–Li neighbors, which might also be a factor for the observed high conductivity.[18]

Furthermore, as mentioned before, amorphization – or a higher degree of disorder in the system – is very beneficial for conductivity. Although $Li_{27-x}[P_4O_{7+x}N_{9-x}]O_3$ is undoubtedly a crystalline compound, there is a significant degree of disorder. Firstly, Li sites are only partially occupied, which means that around 93% of Li positions are occupied in a statistical way. Moreover, both the distribution and orientation of $[PO_3N]^{4-}$ and $[PO_2N_2]^{5-}$ are statistical. This statistical occupation of five out of seven atom sites might lead to a smoothening of the overall energy landscape around Li similar to the situation in amorphous structures, allowing higher Li^+ mobility.

Overall, there are several structural factors that are indeed benign for the ionic conductivity. Overall, our findings point us to a lack of understanding of the complex interplay of all of these structural features in LiPON materials.

Conclusion

The new lithium oxonitridophosphate oxide $Li_{27-x}[P_4O_{7+x}N_{9-x}]O_3$ with $x \approx 1.9(3)$ was synthesized from Li_3N, P_3N_5 and Li_2O. The crystal structure consisting of statistically distributed $[PO_2N_2]^{5-}$ and $[PO_3N]^{4-}$ tetrahedra as well as oxide ions has been elucidated by employing a multitude of analytical methods (scXRD,PXRD, MAS NMR, 2D MAS NMR, neutron powder diffraction). The ionic conductivity of 6.6×10^{-8} S cm^{-1} at 25 °C was obtained from impedance spectroscopy and is comparable to that of amorphous a-LiPON.

With various anion species ($[PO_3N]^{4-}$ and $[PO_2N_2]^{5-}$), as well as a partial occupancy of Li positions and mixed occupancy of O/N positions, $Li_{27-x}[P_4O_{7+x}N_{9-x}]O_3$ contains a complex mixture of structural features that influence the ionic conductivity. However, the impact of those various features on the conductivity is not fully understood yet. With further investigation of the conduction mechanism in $Li_{27-x}[P_4O_{7+x}N_{9-x}]O_3$, Li^+ ion conduction processes in LiPON materials might be understood better.

Experimental Section

Synthesis of P_3N_5: P_3N_5 was synthesized according to literature.[48] P_4S_{10} (Acros Organic, >99.8%) was placed in a dry silica glass tube within a silica glass tube. After saturation with NH_3 (Air Liquide, 99.999%) for 4 h, the starting material was heated to 800 °C with a rate of 300 K/h, kept at this temperature for 4 h and cooled with a rate of 300 K/h in NH_3 gas flow. The orange product was then washed with H_2O, EtOH, and acetone, and dried.

Synthesis of $Li_{27-x}[P_4O_{7+x}N_{9-x}]O_3$: All work was performed under Ar atmosphere in a glovebox (Unilab, MBraun, Garching, $O_2<$ 1 ppm, $H_2O<1$ ppm). P_3N_5 (34.7 mg, 0,213 mmol), Li_3N (Rockwood Lithium, 99.99%, 11.1 mg, 0,320 mmol), and Li_2O (Alfa Aesar, 99.5%, 54.1 mg, 1.81 mmol) were added together in a molar 2:4:17 ratio and ground thoroughly in an agate mortar. The mixture was transferred to a dry Ta crucible placed in a silica tube under Ar counterflow. The ampoule was sealed using an oxyhydrogen burner (all gasses: Air Liquide, 99.999%). The silica ampoule was heated with a rate of 300 °C/h, held at 800 °C for 90 h and cooled to room temperature with a rate of 300 °C/h. The light gray product was washed with EtOH (5 mL) under Ar atmosphere.

Single-crystal X-ray diffraction: Single-crystal X-ray diffraction data were obtained using synchrotron radiation with a wavelength of $\lambda = 0.2947$ Å at ESRF beamline ID11. Semiempirical absorption correction was performed with SADABS.[49] The structure was solved with SHELXS using direct methods and refined with SHELXL.[50]

Deposition Number(s) 2204799, 2204800 contain(s) the supplementary crystallographic data for this paper. These data are provided free of charge by the joint Cambridge Crystallographic Data Centre and Fachinformationszentrum Karlsruhe Access Structures service.

Powder X-ray diffraction: The product was sealed into a glass capillary (Ø = 0.5 mm, wall thickness 0.1 mm, Hilgenberg GmbH) and investigated using a Stoe STADI P diffractometer with Cu $K_{\alpha1}$ radiation ($\lambda = 1.5406$ Å), Ge(111) monochromator and a Mythen 1 K detector in parafocusing Debye–Scherrer geometry. Rietveld refinements were performed using TOPAS 6.[51–53]

For temperature-dependent powder X-ray data, Mo $K_{\alpha1}$ radiation ($\lambda = 0.70930$ Å) with a Ge(111) monochromator was used to record data with a Stoe STADI P and an image plate position sensitive detector. Patterns were recorded in steps of 20 K, starting from room temperature up to 1000 °C with a heating rate of 15 K min^{-1}.

Solid-state magic angle spinning (MAS) NMR methods: NMR data for ^1H, ^6Li, ^7Li, and ^{31}P were obtained using a DSX Advance spectrometer (Bruker). The sample was packed into a rotor (Ø = 2.5 mm), mounted on a commercial MAS probe (Bruker) and spun with a frequency of 25 kHz. The obtained data was analyzed using device-specific software.[54]

Neutron powder diffraction: The product was packed in a vanadium container (Ø = 3 mm) with an indium seal to protect the sample against humidity in the atmosphere. Neutron powder diffraction data has been collected at the instrument SPODI at the neutron source FRM II (Garching b. München, Germany) within a Rapid Access Program.[55] The measurement was performed in Debye-Scherrer geometry with an incident neutron beam having a rectangular cross section of 40×20 mm at the sample position. Monochromatic neutrons with a wavelength of 1.54832(4) Å were chosen from the 5 5 1 reflection of a vertically focused composite Ge monochromator. High resolution neutron powder diffraction data were collected over a 2θ range from 1.0–151.9° using a detector consisting from 80 position-sensitive ^3He counting tubes covering an angular range of 2 $\theta = 160°$ and an effective height of 300 mm was used. The obtained data were analyzed and Rietveld refinements were performed using the program package TOPAS-Academic.[51]

Fourier-transform infrared (FTIR) spectroscopy: FTIR measurements were performed at a Bruker FTIR Alpha II compact spectrometer equipped with a diamond ATR unit. The powder was measured under Ar atmosphere. The spectrum was measured from 400–4000 cm^{-1}.

Elemental analysis: Energy-dispersive X-ray (EDX) spectra were taken at a Dualbeam Helios Nanolab G3 UC (FEI) scanning electron microscope (SEM) featuring an EDX detector (X-Max 80 SDD, Oxford instruments). The sample was placed onto an adhesive carbon pad and coated with a conducting carbon film using a high-vacuum sputter coater (BAL-TEC MED 020, Bal Tec A).

Inductively coupled plasma optical emission spectroscopy (ICP-OES): A Varian Vista RL with a 40 MHz RF generator was used with a VistaChip CCD detector to measure ICP-OES.

Combustion spectroscopy: A Vario MICRO Cube device (Elementar, Langenselbold, Germany) was used to measure the weight percentages of C, H, N, and S.

Determination of partial ionic and electronic conductivity: Electrochemical impedance spectroscopy and potentiostatic polarization measurements were performed with an Ivium compactstat.h (24 bit instrument) in a two-electrode setup using an rhd instruments Microcell HC cell stand loaded with rhd instruments TSC Battery cells. The samples were ground thoroughly and compacted to a pellet of about 0.5–1.0 mm thickness and 5 mm in diameter by uniaxial cold pressing (1000 MPa). The pellets showed relative densities of 80±5%. The pellets were sputtered with ruthenium as ion-blocking electrodes on both sides. The spectra were recorded in a frequency range of 1 MHz–0.01 Hz and an AC voltage of 100 mV was applied. Each sample was measured for several temperature cycles between −5 and 85 °C with 5 °C steps inside a glovebox under argon atmosphere. Analysis of the impedance spectra was carried out with the RelaxIS3 software from rhd instruments. Linearity, stability and causality were checked by the Kramers–Kronig relation before fitting the data. The samples were subsequently used for potentiostatic polarization measurements to extract the electronic partial conductivity at 25 °C. For these a voltage of 0.25, 0.50, 0.75 and 1.00 V was applied for 5–10 h each and the drop in resulting current measured. The resistance was calculated from the current measured at a steady state after several hours.

Acknowledgements

The authors thank Dr. Lisa Gamperl, Christian Minke, and Sandra Albrecht for EDX, NMR, and ICP measurements (all at Department of Chemistry, LMU Munich). Financial support by the DFG under Germany's Excellence Strategy - EXC 2089/1-390776260

(e-conversion) and as part of the grant OE530/6-1 is gratefully acknowledged. A.H. and B.V.L. acknowledge financial support by the German Federal Ministry of Research and Education (BMBF), project 03XP0177B (FestBatt). We thank the ESRF (Grenoble, France) for granting beamtime (experiment CH-6412); Dr. Vadim Dyadkin, Dr. Peter Schultz, Dr. Stefan Schwarzmüller and Dr. Frank Heinke are acknowledged for support during the beamtime. We also thank the FRM II (Munich, Germany) for rapid access beamtime (proposal no. 16528). Open Access funding enabled and organized by Projekt DEAL.

Conflict of Interest

The authors declare no conflict of interest.

Data Availability Statement

The data that support the findings of this study are available in the supplementary material of this article.

Keywords: conducting materials · lithium · neutron diffraction · NMR spectroscopy · solid-state structures

[1] H.-O. Mulfinger, *J. Am. Ceram. Soc.* **1966**, *49*, 462–467.
[2] R. E. Loehman, *J. Non-Cryst. Solids* **1980**, *42*, 433–445.
[3] R. E. Loehman, *J. Non-Cryst. Solids* **1983**, *56*, 123–134.
[4] M. R. Reidmeyer, D. E. Day, *J. Am. Ceram. Soc.* **1985**, *68*, C-188–C-190.
[5] T. M. Holmes, G. L. Leatherman, T. El-Korchi, *J. Mater. Res.* **1991**, *6*, 152–158.
[6] M. R. Reidmeyer, D. E. Day, *J. Non-Cryst. Solids* **1995**, *181*, 201–214.
[7] R. Marchand, *J. Non-Cryst. Solids* **1983**, *56*, 173–178.
[8] R. W. Larson, D. E. Day, *J. Non-Cryst. Solids* **1986**, *88*, 97–113.
[9] J. B. Bates, N. J. Dudney, G. R. Gruzalski, R. A. Zuhr, A. Choudhury, C. F. Luck, J. D. Robertson, *Solid State Ionics* **1992**, *53–56*, 647–654.
[10] S. D. Jones, J. R. Akridge, F. K. Shokoohi, *Solid State Ionics* **1994**, *69*, 357–368.
[11] J. B. Bates, N. J. Dudney, B. Neudecker, A. Ueda, C. D. Evans, *Solid State Ionics* **2000**, *135*, 33–45.
[12] J. F. Ribeiro, R. Sousa, J. P. Carmo, L. M. Gonçalves, M. F. Silva, M. M. Silva, J. H. Correia, *Thin Solid Films* **2012**, *522*, 85–89.
[13] B. C. Bunker, D. R. Tallant, C. A. Balfe, R. J. Kirkpatrick, G. L. Turner, M. R. Reidmeyer, *J. Am. Ceram. Soc.* **1987**, *70*, 675–681.
[14] D. E. Day, *J. Non-Cryst. Solids* **1989**, *112*, 7–14.
[15] N. Mascaraque, A. Durán, F. Muñoz, G. Tricot, *Int. J. Appl. Glas. Sci.* **2016**, *7*, 69–79.
[16] M. A. T. Marple, T. A. Wynn, D. Cheng, R. Shimizu, H. E. Mason, Y. S. Meng, *Angew. Chem. Int. Ed.* **2020**, *59*, 22185–22193; *Angew. Chem.* **2020**, *132*, 22369–22377.
[17] F. Munõz, J. Ren, L. Van Wüllen, T. Zhao, H. Kirchhain, U. Rehfuß, T. Uesbeck, *J. Phys. Chem. C* **2021**, *125*, 4077–4085.
[18] V. Lacivita, N. Artrith, G. Ceder, *Chem. Mater.* **2018**, *30*, 7077–7090.
[19] A. Le Sauze, L. Montagne, G. Palavit, F. Fayon, R. Marchand, *J. Non-Cryst. Solids* **2000**, *263–264*, 139–145.
[20] C. Dietrich, M. Sadowski, S. Sicolo, D. A. Weber, S. J. Sedlmaier, K. S. Weldert, S. Indris, K. Albe, J. Janek, W. G. Zeier, *Chem. Mater.* **2016**, *28*, 8764–8773.
[21] S. Schneider, L. G. Balzat, B. V. Lotsch, W. Schnick, *Chem. Eur. J.* **2023**, *29*, e202202984.
[22] B. Wang, B. C. Chakoumakos, B. C. Sales, B. S. Kwak, J. B. Bates, *J. Solid State Chem.* **1995**, *115*, 313–323.
[23] K. Senevirathne, C. S. Day, M. D. Gross, A. Lachgar, N. A. W. Holzwarth, *Solid State Ionics* **2013**, *233*, 95–101.
[24] D. Baumann, W. Schnick, *Eur. J. Inorg. Chem.* **2015**, 617–621.
[25] P. López-Aranguren, M. Reynaud, P. Głuchowski, A. Bustinza, M. Galceran, J. M. López Del Amo, M. Armand, M. Casas-Cabanas, *ACS Energy Lett.* **2021**, *6*, 445–450.
[26] A. Al-Qawasmeh, N. A. W. Holzwarth, *J. Power Sources* **2017**, *364*, 410–419.
[27] E.-M. Bertschler, C. Dietrich, J. Janek, W. Schnick, *Chem. Eur. J.* **2017**, *23*, 2185–2191.
[28] E.-M. Bertschler, R. Niklaus, W. Schnick, *Chem. Eur. J.* **2017**, *23*, 9592–9599.
[29] E.-M. Bertschler, T. Bräuniger, C. Dietrich, J. Janek, W. Schnick, *Angew. Chem. Int. Ed.* **2017**, *56*, 4806–4809; *Angew. Chem.* **2017**, *129*, 4884–4887.
[30] E.-M. Bertschler, R. Niklaus, W. Schnick, *Chem. Eur. J.* **2018**, *24*, 736–742.
[31] E.-M. Bertschler, C. Dietrich, T. Leichtweiß, J. Janek, W. Schnick, *Chem. Eur. J.* **2018**, *24*, 196–205.
[32] Y. Deng, C. Eames, J. N. Chotard, F. Laleìre, V. Seznec, S. Emge, O. Pecher, C. P. Grey, C. Masquelier, M. S. Islam, *J. Am. Chem. Soc.* **2015**, *137*, 9136–9145.
[33] R. D. Shannon, *Acta Crystallogr.* **1976**, *A32*, 751–767.
[34] S. D. Kloß, O. Janka, T. Block, R. Pöttgen, R. Glaum, W. Schnick, *Angew. Chem. Int. Ed.* **2019**, *58*, 4685–4689; *Angew. Chem.* **2019**, *131*, 4733–4737.
[35] W. Schnick, J. Luecke, *J. Solid State Chem.* **1990**, *87*, 101–106.
[36] N. I. P. Ayu, E. Kartini, L. D. Prayogi, M. Faisal, Supardi, *Ionics* **2016**, *22*, 1051–1057.
[37] T. Ben-Chaabane, L. Smiri-Dogguy, Y. Laligant, A. Le Bail, *Eur. J. Solid State Inorg. Chem.* **1998**, *35*, 255–264.
[38] E. V. Murashova, N. N. Chudinova, *Crystallogr. Rep.* **2001**, *46*, 942–947.
[39] V. I. Voronin, E. A. Sherstobitova, V. A. Blatov, G. S. Shekhtman, *J. Solid State Chem.* **2014**, *211*, 170–175.
[40] K. Nakamoto, *Infrared and Raman Spectra of Inorganic and Coordination Compounds: Part A: Theory and Applications in Inorganic Chemistry: Sixth Edition*, John Wiley & Sons, Inc., Hoboken, NJ, **2008**.
[41] M. A. Carrillo Solano, M. Dussauze, P. Vinatier, L. Croguennec, E. I. Kamitsos, R. Hausbrand, W. Jaegermann, *Ionics* **2016**, *22*, 471–481.
[42] J. T. S. Irvine, D. C. Sinclair, A. R. West, *Adv. Mater.* **1990**, *2*, 132–138.
[43] S. Zhao, Z. Fu, Q. Qin, *Thin Solid Films* **2002**, *415*, 108–113.
[44] S. Lorger, R. Usiskin, J. Maier, *J. Electrochem. Soc.* **2019**, *166*, A2215–A2220.
[45] J. Li, W. Lai, *Solid State Ionics* **2020**, *351*, 115329.
[46] Y. A. Du, N. A. W. Holzwarth, *Phys. Rev. B* **2007**, *76*, 174302.
[47] H. Rabaâ, R. Hoffmann, N. Cruz Hernández, J. Fernandez Sanz, *J. Solid State Chem.* **2001**, *161*, 73–79.
[48] A. Stock, B. Hoffmann, *Ber. Dtsch. Chem. Ges.* **1903**, *36*, 314–319.
[49] Bruker, *SADABS*, Bruker AXS Inc., Madison, WI, USA, **2009**.
[50] G. M. Sheldrick, *Acta Crystallogr. Sect. C* **2015**, *71*, 3–8.
[51] A. A. Coelho, *TOPAS Academic Version 6*, Coelho Software, Brisbane, Australia, **2016**.
[52] R. W. Cheary, A. A. Coelho, *J. Appl. Crystallogr.* **1992**, *25*, 109–121.
[53] R. W. Cheary, A. A. Coelho, J. P. Cline, *J. Res. Natl. Inst. Stan.* **2004**, *109*, 1–25.
[54] Bruker, *Topspin v.3.0 Pl 3*, Bruker Biospin GmbH, Germany, **2010**.
[55] M. Hoelzel, A. Senyshyn, O. Dolotko, *J. large-scale Res. Facil. JLSRF* **2015**, *1*, 18–21.

Manuscript received: January 17, 2023
Accepted manuscript online: February 21, 2023
Version of record online: March 24, 2023